TEST CASE DOCUMENTATION AND TESTING RESULTS

TEST CASE ID ICFD-VAL-2.1

Backward facing Step

Tested with LS-DYNA® v980 Revision Beta

Friday 1st June, 2012

LSTC
Livermore Software Technology Corp.

Document Information	
Confidentiality	**external use**
Document Identifier	LSTC-QA-LS-DYNA-ICFD-VAL-2.1-1
Author(s)	Iñaki Çaldichoury, Facundo Del Pin
Number of pages	23
Date created	Friday 1st June, 2012
Distribution	External

Disclaimer:

The test case(s) described herein are for illustrative purposes only. LSTC does not warrant that a user of these or other LS-DYNA features will experience the same or similar results or that a feature will meet the user's particular requirements or operate error free. FURTHERMORE, THERE ARE NO WARRANTIES, EITHER EXPRESS OR IMPLIED, ORAL OR WRITTEN, WITH RESPECT TO THE DOCUMENTATION AND SOFTWARE DESCRIBED HEREIN INCLUDING, BUT NOT LIMITED TO ANY IMPLIED WARRANTIES (i) OF MERCHANTABILITY, OR (ii) FITNESS FOR A PARTICULAR PURPOSES, OR (iii) ARISING FROM COURSE OF PERFORMANCE OR DEALING, OR FROM USAGE OF TRADE OR. THE REMEDIES SET FORTH HEREIN ARE EXCLUSIVE AND IN LIEU OF ALL OTHER REMEDIES FOR BREACH OF WARRANTY.

Contents

1 Introduction

1.1 Purpose of this Document

This document specifies the test case ICFD-VAL-2.1. It provides general test case information like name and ID as well as information to the confidentiality, status, and classification of the test case.

A detailed description of the test case is given, the purpose of the test case is defined, and the tested features are named. Results and observations are stated and discussed. Testing results are provided in section 4.1 for the therein mentioned LS-DYNA® version and platforms.

2 Test Case Information

Test Case Summary	
Confidentiality	external use
Test Case Name	Backward facing Step: 2D parabolic flow suddenly expanding
Test Case ID	ICFD-VAL-2.1
Test Case Status	Under consideration
Test Case Classification	Validation
Metadata	INTERNAL FLOW

Table 1: Test Case Summary

3 Test Case Specification

3.1 Test Case Purpose

The phenomenon of boundary layer separation and reattachment is frequently encountered in fluid mechanics and is of practical and theoretical interest. Numerical methods aim to solve and correctly reproduce such complex phenomena. The purpose of this test case will be to study the flow over a backward facing step focusing on the reattachment and separation zones.

3.2 Test Case Description

The flow over a backward-facing step is found in a variety of engineering applications involving flows in ducts or channels in order for instance to create a recirculation zone of a sudden change in pressure. The fact that the problem's geometry is rather simple while retaining rich flow physics manifested by flow separation, flow reattachment and multiple recirculating bubbles in the channel depending on the Reynolds number and geometrical parameters such as the step height, the channel height and the presence or not of an inlet channel has made this problem a classical numerical problem.

A simple sketch of the problem is shown in Figure (1). The reference Reynolds number is taken as :

$$Re = \frac{\rho h_i V}{\nu} \tag{1}$$

with ρ the fluid's density, h_i the characteristic length of the problem i.e the inlet channel height, V the average incoming velocity ($\frac{2}{3}V_{max}$) and ν the fluid's viscosity.

For this study, the Reynolds number will be varied from 100 to 1200 thus going from the laminar regime to possibly reaching the transient regime ([1] and [4]).

The chosen length of the inlet channel is based on the results of [2] which show that for a inlet parabolic profile, the variation of the results become minimal after the length of the inlet channel becomes bigger than 2. The length of the outflow channel has been chosen long enough so that a fully developed Poiseuille flow can be observed at the outlet after convergence of the analysis.

For this test case, two sets of experimental references will be used. The first reference by [1] is the one most commonly used with experimental results obtained by laser-Doppler velocimetry with frequently shifting and with an expansion ratio (i.e $\frac{H}{h_i}$) of 1.94. An expansion ratio of 2 will also be used in order to compare the results with the experimental results of [4] obtained by multi-element hot-film sensor (MHFS) arrays, in conjunction with a bank of

constant-temperature anemometers. Finally [3], which provides very complete numerical results for both expansion ratios of 1.94 and 2 will be used as the main reference for numerical results.

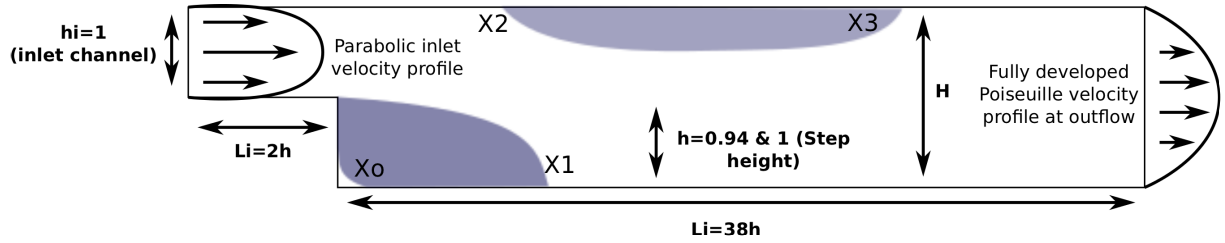

Figure 1: Sketch of the backward-facing step

The main objective of this test case is to study the reattachment and separation lengths x_0, x_1, x_2, and x_3 as shown in Figure (1) and to compare the results with both experimental references and numerical references. This analysis will be divided in three phases for both expansion ratios of 1.94 and 2. During the first phase, the Reynolds number will be varied from 100 to 600. The results and observations made during this phase will assist in the setting up of the model used for the second phase where the Reynolds number will be varied from 500 to 900. Finally, the results obtained during the second phase will assist in the setting up of the third phase with the Reynolds number varying from 800 to 1200.

3.3 Model Description-Phase 1

A complete description of the model's mesh sizes used for phase one is depicted in Table (2). A zoom of the resulting volume mesh close to the step after running the test case is shown in Figure (2). Table (3) gives the physical parameters that will be used with the viscosity values depending on the Reynolds number.

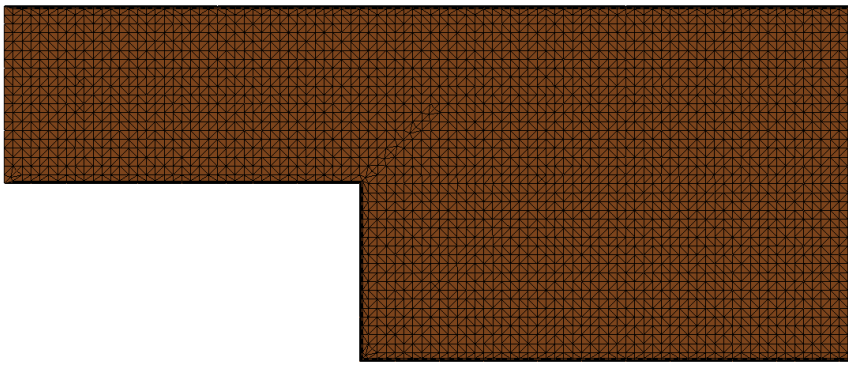

Figure 2: Test Case Mesh-Phase One

Model information	
Surface element size	0.05
Volume Nodes	36911
Volume Elements	72140
Anisotropic Elements added to the Boundary Layer	2

Table 2: Model meshing parameters-Phase One

Model physical parameters	
Incoming Maximum Velocity	1
Fluid Density	1
Fluid Viscosity	0.0133 to 0.00222

Table 3: Test Case Parameters-Phase One

3.4 Model Description-Phase 2

For this phase four zones will be defined each one of them with a distinct mesh size (see Figure (3)). The first zone corresponding to the inlet will retain the original surface element mesh size. For zone two, which corresponds to the location of x_1, x_2 and x_3, the surface element mesh size will be divided by two. Zone 3 corresponds to a transitional zone where the surface element mesh size is equal to the phase one mesh size while zone 4 has a two times coarser mesh in order to save some computational time. Figure (4) shows the volume mesh at the different zone junctions and Table (5) offers a summary of the chosen element sizes for the different zones.

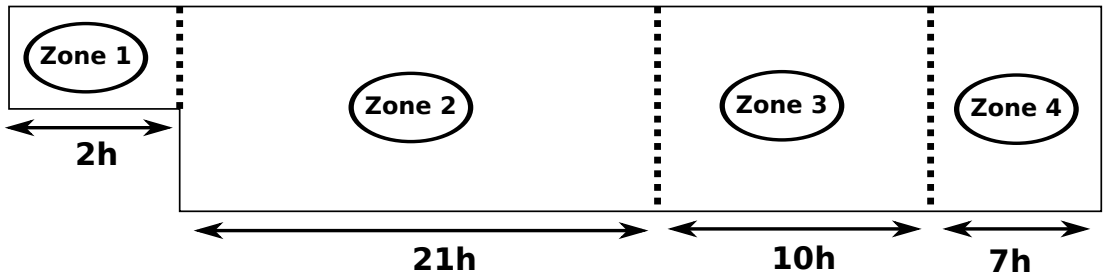

Figure 3: Mesh size zones sketch-Phase Two

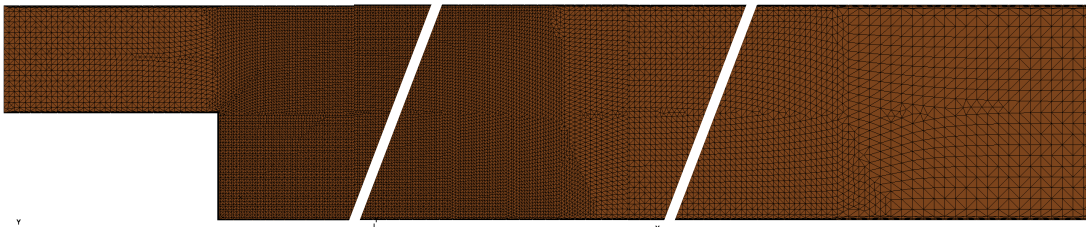

Figure 4: Test Case Mesh-Phase Two

Model information	
Zone 1 & 3-Surface element size	0.05
Zone 2-Surface element size	0.025
Zone 4-Surface element size	0.1
Volume Nodes	85274
Volume Elements	168159
Anisotropic Elements added to the Boundary Layer	2

Table 4: Model meshing parameters-Phase Two

Model physical parameters	
Incoming Maximum Velocity	1
Fluid Density	1
Fluid Viscosity	0.002666 to 0.0014813

Table 5: Test Case Parameters-Phase Two

3.5 Model Description-Phase 3

For this phase a finer surface element mesh is defined in the area where the expected upper boundary layer separation, x_2 will occur (Zone 5 in Figure (5)) dividing the former Zone 2 in two parts. Due to the expected increase of x_3, Zone 2b is extended compared to phase 2 and there is no longer any surface element mesh size corresponding to Zone 4. Figure (6) shows the volume mesh at the junction between Zone 2a and the newly created Zone 5. Table (6) offers a summary of the chosen element sizes for the different zones. Table (7) gives the physical parameters that will be used with the viscosity values depending on the Reynolds number.

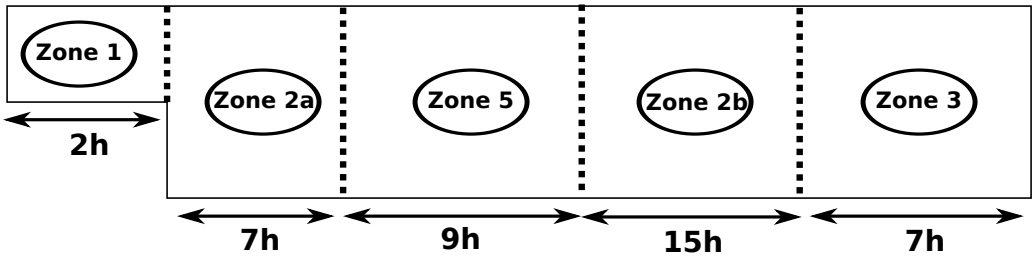

Figure 5: Mesh size zones sketch-Phase Three

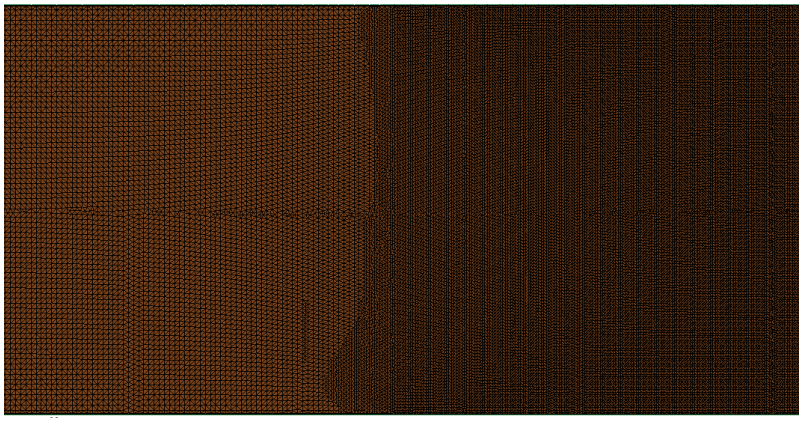

Figure 6: Test Case Mesh-Phase Three

Model information	
Zone 1-Surface element size	0.05
Zone 2a & 2b-Surface element size	0.025
Zone 3-Surface element size	0.05
Zone 5-Surface element size	0.0125
Volume Nodes	201964
Volume Elements	400266
Anisotropic Elements added to the Boundary Layer	2

Table 6: Model meshing parameters-Phase Three

Model physical parameters	
Incoming Maximum Velocity	1
Fluid Density	1
Fluid Viscosity	0.0014813 to 0.001111

Table 7: Test Case Parameters-Phase Three

4 Test Case Results

4.1 Results and discussion-Phase 1

Figure (7) and (8) show the velocity fringes for the Reynolds numbers of 100 and 600. The bottom recirculation zone expanding between these two Reynolds numbers can be observed. The upper recirculation zone has also appeared and can be clearly identified for $Re = 600$. Table (8) offers a summery of the different reattachment and separation lengths found for the Reynolds number ranging from 100 to 600. Those results are used to plot Figure (9) and (10) where a comparison with reference numerical and experimental results can be made.

Comparison with reference experimental results : In both cases, the present analysis results follow the global behavior of the experimental reference results. A better agreement is found with the more recent results by [4] and $ER = 2$ especially for the lower bottom x_1 reattachment length.

Comparison with reference numerical results : For both expansion ratios, Figure (9) and (10) show a good agreement for x_1 until $Re = 500$ between the numerical results obtained by [3] and the present analysis. For $Re = 500$ and $Re = 600$, the beginning of a slight divergence of the results can be observed. For both expansion rations, x_2 follows the same behavior as the results given by [3] but is slightly underestimated in each case. For both expansion ratios, x_3 agrees pretty well with the results given by [3] and no further observation can be made. The slight divergence starting at $Re = 500$ for x_1 and the systematic underestimation of x_2 justifies the need for a finer mesh around the reattachment and separation zones for $Re > 500$. This will be the object of Phase Two.

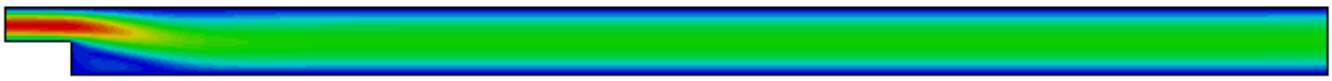

Figure 7: Test Case velocity fringes for $ER = 2$ and $Re = 100$

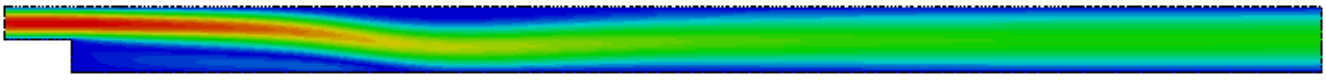

Figure 8: Test Case velocity fringes for $ER = 2$ and $Re = 600$

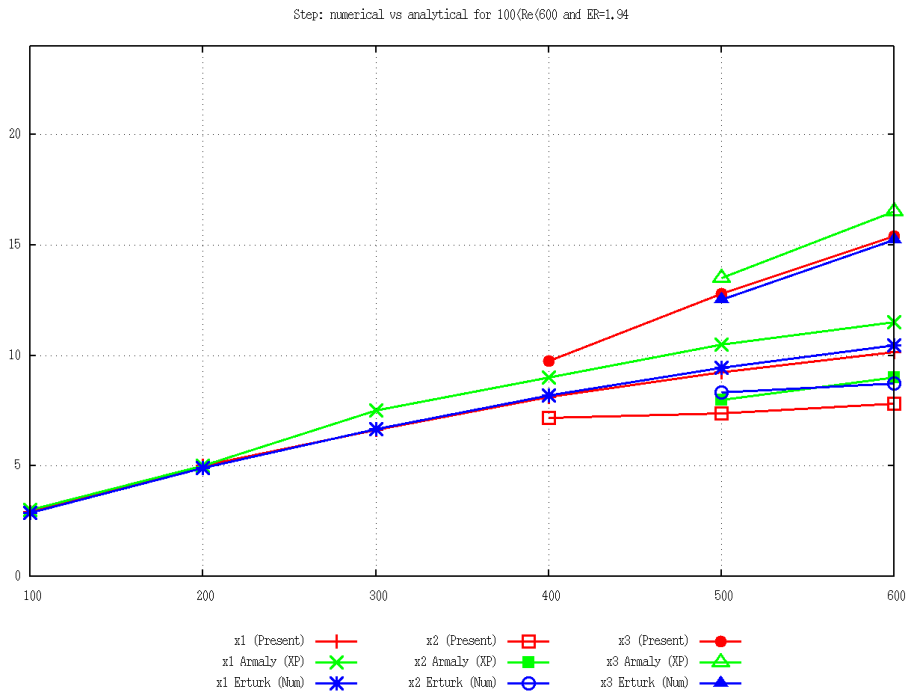

Figure 9: Comparison of x_1, x_2, x_3 for $ER = 1.94$ between present analysis (in red), and reference numerical (in blue, see [3]) and experimental results (in green, see [1]) for $100 \leq Re \leq 600$-Phase one

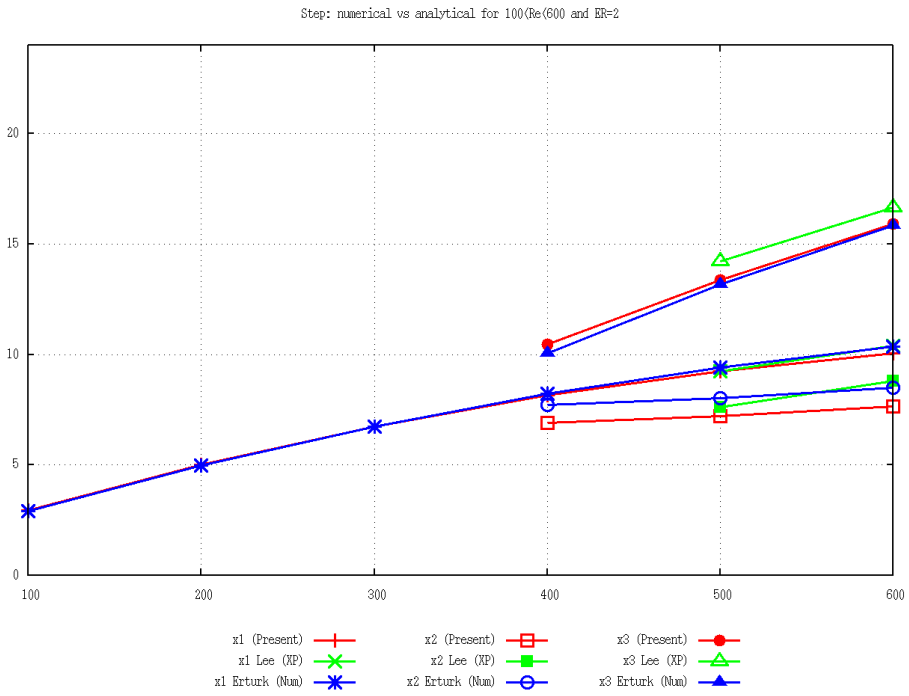

Figure 10: Comparison of x_1, x_2, x_3 for $ER = 2$ between present analysis (in red), and reference numerical (in blue, see [3]) and experimental results (in green, see [4]) for $100 \leq Re \leq 600$-Phase one

Reynolds	ER=1.94			ER=2		
	x_1/h	x_2/h	x_3/h	x_1/h	x_2/h	x_3/h
100	2.92			2.95		
200	4.99			5		
300	6.63			6.75		
400	8.12	7.16	9.76	8.15	6.9	10.45
500	9.23	7.37	12.79	9.25	7.20	13.35
600	10.13	7.80	15.39	10.05	7.65	15.90

Table 8: Numerical results for separation and reattachment positions-Phase One

4.2 Results and discussion-Phase 2

Table (9) shows the results obtained for phase two. Figure (11) and (12) are identical to Figure (9) and (10) but use the results obtained during Phase 2 for the Reynolds number of 500 and 600. It can be seen that the x_2 upper separation length values have moved closer to the reference numerical results of [3]. This can be clearly identified through the change of slope of the x_2 curves between the Reynolds value of 400 which has been computed during phase one and the newly computed result for the Reynolds value of 500. The slight divergence for the x_1 reattachment length that was beginning to appear for the Reynolds value of 500 between the present analysis and the results of [3] has also disappeared. Figure (13) and (14) show the complete curves obtained using the results of phase one for a Reynolds number up to 400 and using the results of phase two for a Reynolds number up to 900. The results retain a coherent behavior with the experimental results and remain in good agreement with the numerical results of [3]. Phase three will consist in confirming these results for a Reynolds number up to 1200 and to analyze whether a further convergence towards the results of [3] can be obtained for x_2.

Reynolds	ER=1.94			ER=2		
	x_1/h	x_2/h	x_3/h	x_1/h	x_2/h	x_3/h
500	9.47	7.88	12.84	9.42	7.65	13.42
600	10.45	8.30	15.50	10.32	8.12	16.00
700	11.22	8.75	17.91	11.07	8.60	18.42
800	11.91	9.26	20.13	11.75	9.07	20.67
900	12.55	9.66	22.28	12.40	9.55	22.85

Table 9: Numerical results for separation and reattachment positions-Phase Two

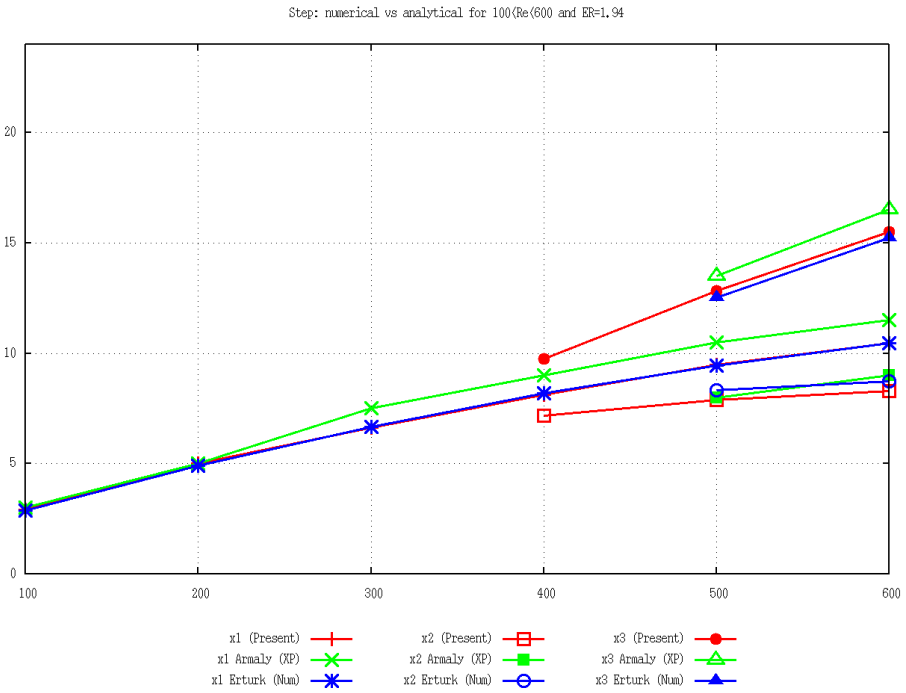

Figure 11: Comparison of x_1, x_2, x_3 for $ER = 1.94$ between present analysis (in red), and reference numerical (in blue, see [3]) and experimental results (in green, see [1])for $100 \leq Re \leq 600$-Phase two

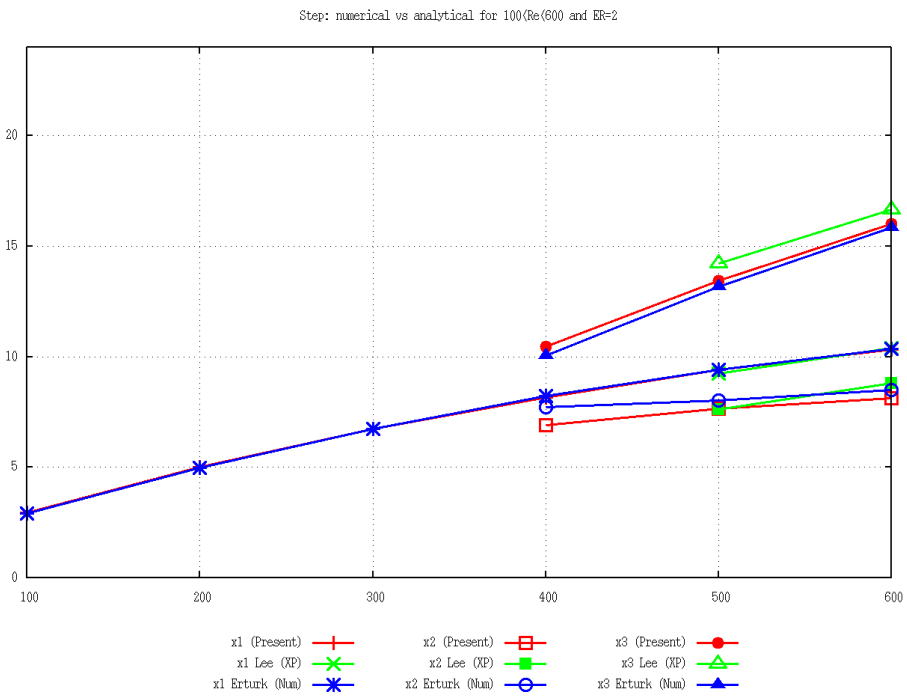

Figure 12: Comparison of x_1, x_2, x_3 for $ER = 2$ between present analysis (in red), and reference numerical (in blue, see [3]) and experimental results (in green, see [4])for $100 \leq Re \leq 600$-Phase two

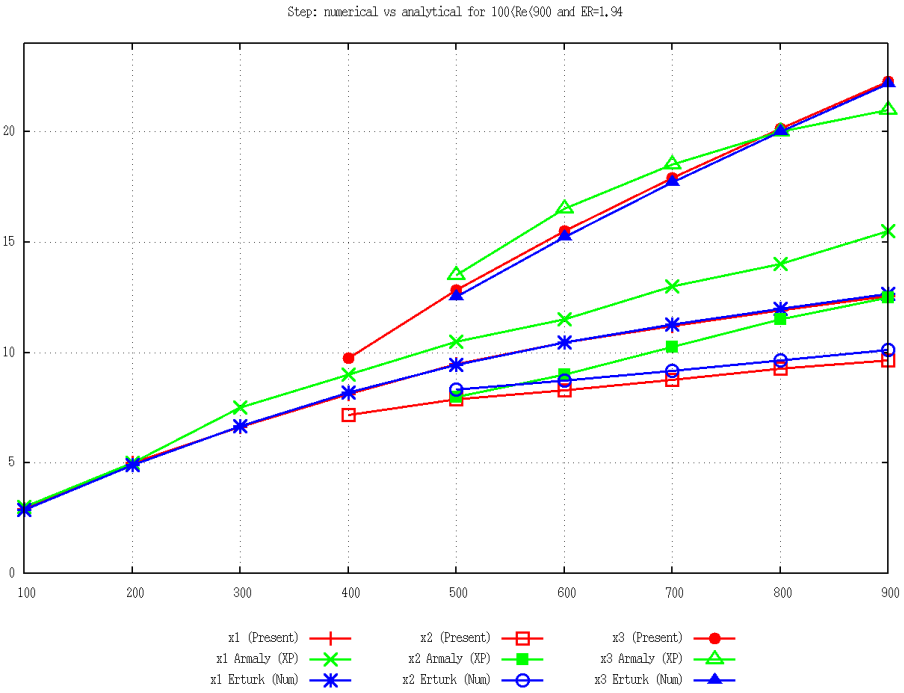

Figure 13: Comparison of x_1, x_2, x_3 for $ER = 1.94$ between present analysis (in red), and reference numerical (in blue, see [3]) and experimental results (in green, see [1])for $100 \leq Re \leq 900$-Phase two

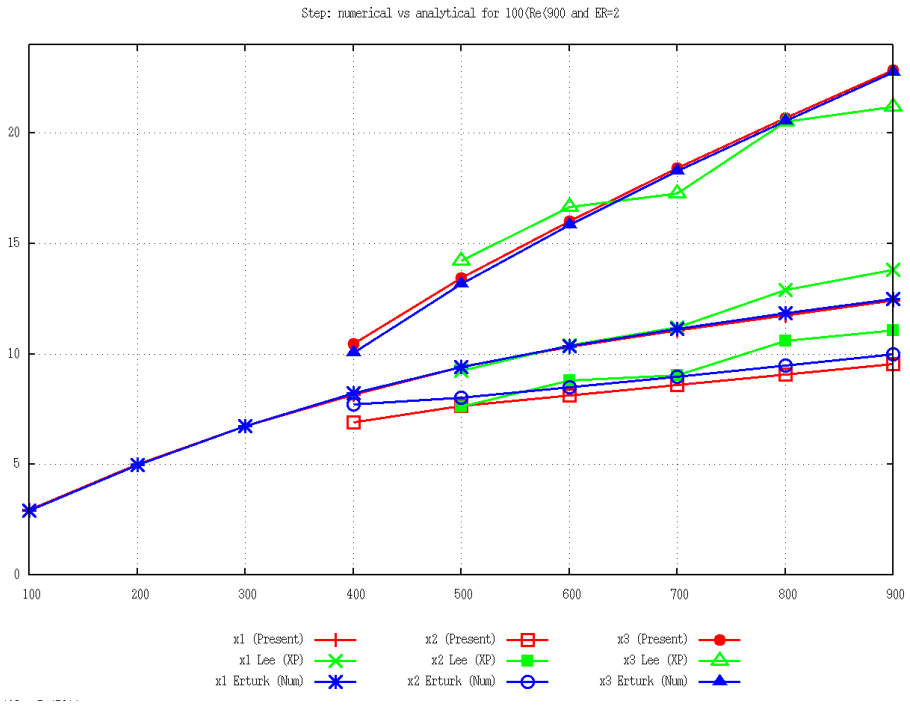

Figure 14: Comparison of x_1, x_2, x_3 for $ER = 2$ between present analysis (in red), and reference numerical (in blue, see [3]) and experimental results (in green, see [4])for $100 \leq Re \leq 900$-Phase two

4.3 Results and discussion-Phase 3

Table (10) shows the results obtained for phase three. Figure (15) and (14) show the final values obtained using the results of Phase One for a Reynolds number up to 400, the results of Phase Two for a Reynolds number up to 800 and the results of Phase Three for a Reynolds number up to 1200. The convergence of the x_2 value to the results of [3] when refining the mesh is confirmed through the change of slope that can be identified between the Reynolds number of 800 and 900. The average deviation between the results of [3] and the present analysis for x_2 for the three phases is summed up in Table (11) and shows the mesh grid convergence rate. Figure (17) shows the influence of the expansion ratio on the results for x_1, exposing similar results with those of [3]. A greater length of x_1 for an expansion number of 2 up to a Reynolds number of 400 and a greater length for an 1.942 expansion ratio for a Reynolds number greater then 400 can be observed.

As a conclusion, it can be stated that even if the results start to differ compared to experimental results when reaching higher Reynolds numbers, possibly due to turbulent effects that start to appear, the global behavior is retained and the results are in very good agreement with the reference numerical values of [3].

Reynolds	ER=1.94			ER=2		
	x_1/h	x_2/h	x_3/h	x_1/h	x_2/h	x_3/h
900	12.65	9.87	22.36	12.5	9.76	22.90
1000	13.29	10.36	24.41	13.15	10.26	25.00
1100	13.90	10.85	26.50	13.75	10.76	27.00
1200	14.47	11.32	28.44	14.37	11.26	29.09

Table 10: Numerical results for separation and reattachment positions-Phase Three

Phase	ER=1.94	ER=2
1	10.96%	10.32%
2	4.71%	4.31%
3	1.34%	2.03%

Table 11: Average deviation from the results of [3] for the x_2 value for the three phases

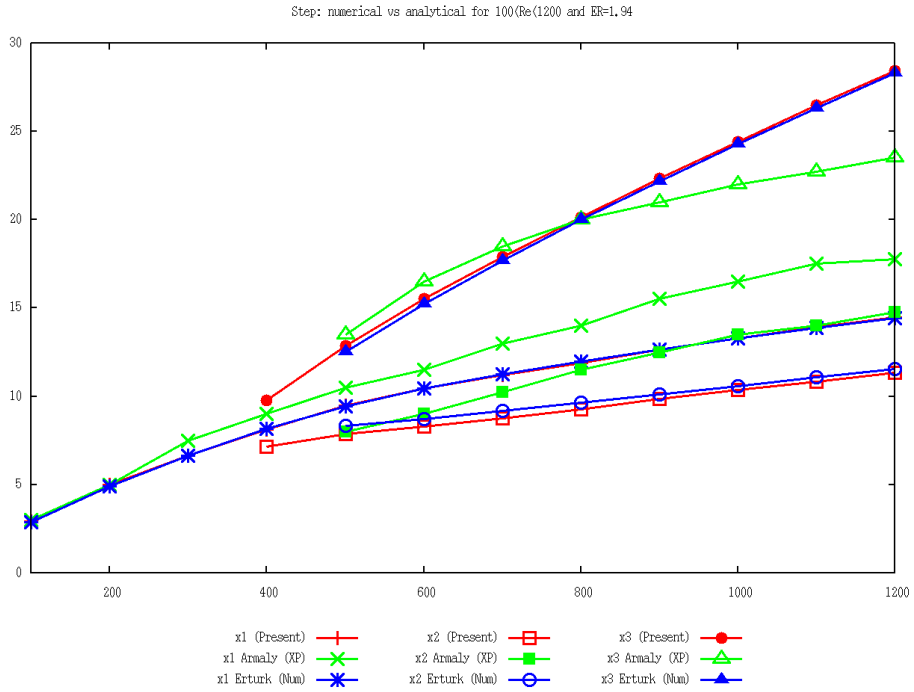

Figure 15: Comparison of x_1, x_2, x_3 for $ER = 1.94$ between present analysis (in red), and reference numerical (in blue, see [3]) and experimental results (in green, see [1])for $100 \leq Re \leq 600$-Phase three

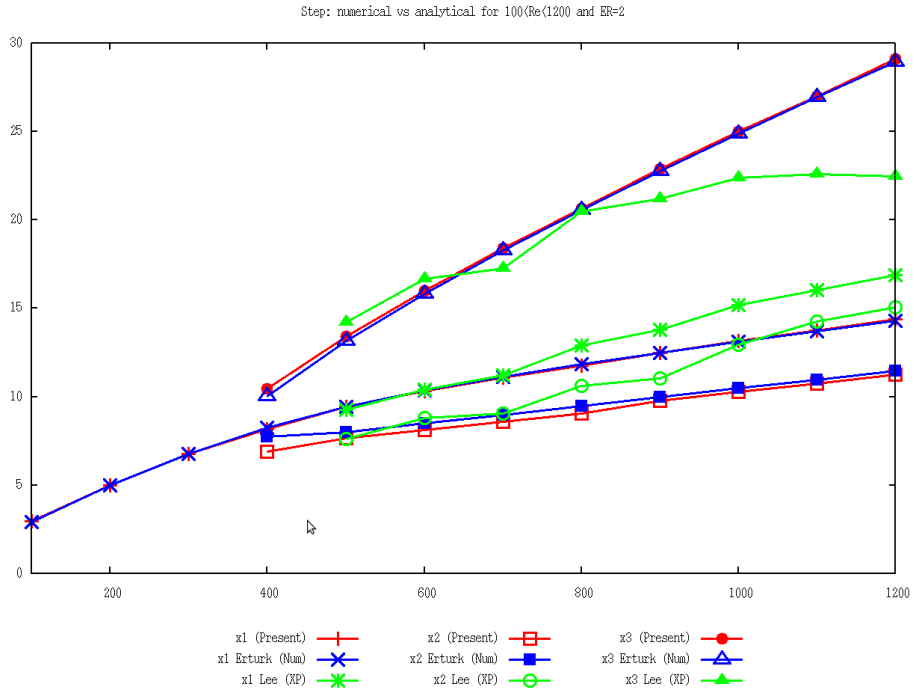

Figure 16: Comparison of x_1, x_2, x_3 for $ER = 2$ between present analysis (in red), and reference numerical (in blue, see [3]) and experimental results (in green, see [4])for $100 \leq Re \leq 600$-Phase three

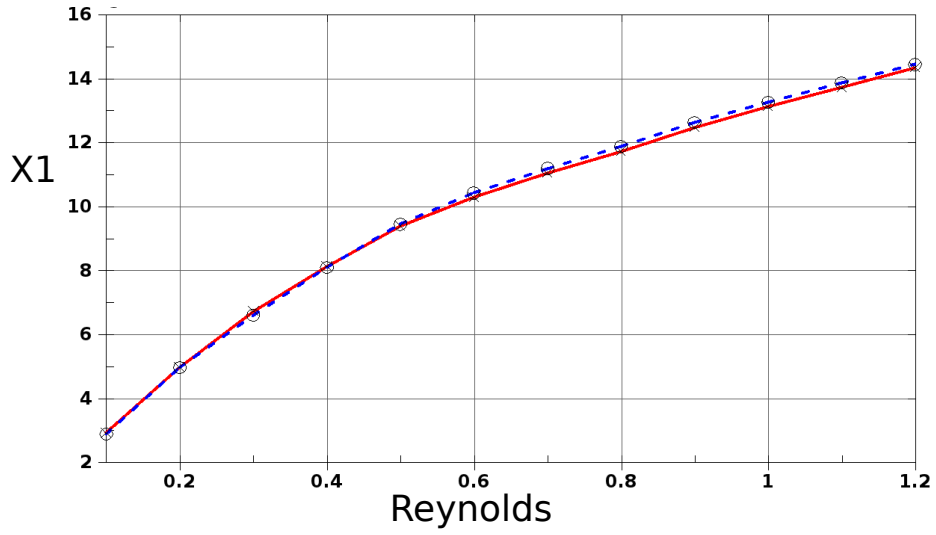

Figure 17: Influence of the Expansion ratio on the results for x_1 (ER=2 in red and ER=1.92 in blue, dashed)

References

[1] J. C. F. P. B. F. ARMALY, F. DURST AND B. SCHONUNG, *Experimental and theoretical investigation of backward-facing step flow*, Fluid Mech, 127 (1982), pp. 473–496.

[2] I. E. BARTON, *The entrance effect of laminar flow over a backward-facing step geometry*, International journal for numerical methods in fluids, 25 (1997), pp. 633–644.

[3] E. ERTURK, *Numerical solutions of 2-d steady incompressible flow over a backward-facing step, part i: High reynolds number solutions*, International journal for numerical methods in fluids, 60 (2009), pp. 275–294.

[4] T. LEE AND D. MATEESCU, *Experimental and numerical investigation of 2-d backkward facing step flow*, Computers and Fluids, 37 (2008), pp. 633–655.